# Practical guide to characterize biomolecule adsorption on solid surfaces (Review)

Elisa Migliorini, Marianne Weidenhaupt, Catherine Picart

# Practical guide to characterize biomolecule adsorption on solid surfaces (Review)

Elisa Migliorini, Marianne Weidenhaupt, and Catherine Picart

Citation: Biointerphases **13**, 06D303 (2018); doi: 10.1116/1.5045122
View online: https://doi.org/10.1116/1.5045122
View Table of Contents: http://avs.scitation.org/toc/bip/13/6
Published by the American Vacuum Society

# Practical guide to characterize biomolecule adsorption on solid surfaces (Review)

Elisa Migliorini,[1] Marianne Weidenhaupt,[1,2] and Catherine Picart[1,2,a)]
[1]*CNRS UMR 5628 (LMGP), Grenoble 38016, France*
[2]*Grenoble Institute of Technology, Université Grenoble Alpes, LMGP, Grenoble 38031, France*

(Received 17 June 2018; accepted 26 September 2018; published 23 October 2018)

The control over the adsorption or grafting of biomolecules from a liquid to a solid interface is of fundamental importance in different fields, such as drug delivery, pharmaceutics, diagnostics, and tissue engineering. It is thus important to understand and characterize how biomolecules interact with surfaces and to quantitatively measure parameters such as adsorbed amount, kinetics of adsorption and desorption, conformation of the adsorbed biomolecules, orientation, and aggregation state. A better understanding of these interfacial phenomena will help optimize the engineering of biofunctional surfaces, preserving the activity of biomolecules and avoiding unwanted side effects. The characterization of molecular adsorption on a solid surface requires the use of analytical techniques, which are able to detect very low quantities of material in a liquid environment without modifying the adsorption process during acquisition. In general, the combination of different techniques will give a more complete characterization of the layers adsorbed onto a substrate. In this review, the authors will introduce the context, then the different factors influencing the adsorption of biomolecules, as well as relevant parameters that characterize their adsorption. They review surface-sensitive techniques which are able to describe different properties of proteins and polymeric films on solid two-dimensional materials and compare these techniques in terms of sensitivity, penetration depth, ease of use, and ability to perform "parallel measurements." 
https://doi.org/10.1116/1.5045122

## I. INTRODUCTION

The adsorption of proteins and polymers on surfaces plays a crucial role in several domains with growing economic and societal importance. In the biomedical field in particular, a thorough understanding of the adsorption phenomena and a precise control over the surfaces and adsorbed molecules are often keys for a successful application.

### A. Diagnostics

The design of sensitive and robust diagnostic tools, like lateral flow immune chromatographic assays using porous materials, relies on surface-immobilized capture antibodies with a specific orientation.[1] A meticulous control over the amount and conformation of these molecules on the surface guarantees the quality of the diagnostic test.

### B. Pharmaceutics and vaccine production

The dose and structural integrity of biologics is critical for their therapeutic efficiency.[2] During the manufacturing, long-term storage, and administration to patients, therapeutic proteins are exposed to variable surfaces and interfaces to which they adsorb because of their inherent amphiphilic nature.[3] Loss of protein and conformational changes triggered by surface adsorption have therefore to be controlled and minimized with adequate formulation additives.

### C. Tissue engineering

The host response to a biomaterial is critical in the determination of the success of implantable devices. This response is determined first by the proteins that interact with the implant surface and then by the cells present in the extracellular matrix within the biological fluids at the vicinity of the implant. Cells interact foremost with the adsorbed proteins. The nature and the activity of these proteins, once adsorbed, dictate the initial cellular and sequential host response. For instance, the presence of intermolecular aggregates in the bone morphogenetic protein 2 (BMP-2) growth factor may alter its interaction with the cellular receptors BMP receptors, ultimately leading to a loss of biological activity. The consequence of such bioactivity loss is a decrease in biological signaling insight the cell. In case of bone, this may be the case for a loss of biochemical signaling by bone precursor cells, thus impacting their ability to differentiate into bone cells.[4,5]

### D. Biomimetic lipid membranes to study protein–lipid interactions

Biomimetic membranes enable to mimic *in vitro*, in simplified systems, the plasma membrane of cells and to study its interaction with proteins in well-defined conditions.

a)Author to whom correspondence should be addressed: catherine.picart@grenoble-inp.fr

Indeed fixed physicochemical parameters (pH, ionic strength and type of buffer) enable to control membrane formation[6,7] and lipid composition, for example the type and amount of negatively charged lipids like phosphatidylserine or phosphatidyl inositols. Such defined conditions allow then to study the specific roles of the selected lipids in protein/lipid interactions.[8,9] These proteins can be cytosolic (in solution) like the ezrin, radixin, and moesin family of proteins that play a role in the anchorage between the cellular cytoskeleton and the plasma membrane[10,11] or incorporated in the lipid membrane (i.e., integral membrane proteins).[12] The study of protein/lipid interactions is of prime importance in a large number of physiological and pathological processes such as viral and parasite invasion including plasma membrane budding,[8] in the formation of cellular protrusions[13] to orchestrate cytoskeletal deformation and associated biochemical signaling.

The process of protein adsorption onto a surface can be due to (i) spontaneous adsorption induced mainly by electrostatic or hydrophobic interactions with the substrate or (ii) the functionalization of the material with either reactive functional groups (i.e., N-Hydroxysuccinimide-ester) or ligands that bind specifically to the proteins. As a consequence, biomolecules are stabilized on the surface by noncovalent interaction forces (physisorption), by covalent bonding, or via the affinity they have for a particular immobilized ligand. The amount and orientation of the adsorbed molecules as well as the reversibility of the adsorption process are all influenced by the mode of interaction with the surface.[14]

In this review, we focus on the control and characterization of biomolecule adsorption from a liquid solution to a surface, either bare or functionalized. Thus, we will not address the case of nanoparticles in solution,[15] for which the analytical techniques are different. We are also not presenting techniques that are specific to the field of biosensing since here we do not aim to quantify the concentration of analytes in a solution but rather quantify the amount of adsorbed biomolecules on a given surface and how they interact with this surface (kinetics, conformational state). The biomolecules may be proteins, lipids, or polymeric chains that are soluble such as polyelectrolytes or polyethylene glycol (PEG) (Fig. 1). The biomolecules can be covalently attached or noncovalently adsorbed on the surface. Furthermore, we decided to focus solely on proteins or polymers with pharmaceutical value, which are often very expensive and available only in low amounts. We will not discuss model proteins such as bovine serum albumin (BSA) or lysozyme, which are widely studied and have already been reviewed.[16] Here, we describe a toolbox of surface-sensitive techniques that can help scientists to control the adsorption of unlabeled biomolecules at the solid–liquid interface. For each technique, we will highlight the parameters that can be measured as well as its advantages and drawbacks (Table I). Notably, a given experimental technique is often associated to a particular experimental setup, including a flow cell. The configuration of this flow cell is technique-dependent in that there may be some geometrical constraints to guide the physical signals to the sensing surface. Besides, since the studied biomolecules are available only in low amounts, these flow cells are often designed to require only very small volumes (ideally in the $\mu$L range).

To note, another factor not given in Table I may be taken into account by the users: the costs of the consumables and maintenance are not indicated but can greatly impact the global costs of the experiments.

## II. PARAMETERS INFLUENCING BIOMOLECULE SURFACE ADSORPTION

Biomolecule adsorption is mostly studied at the solid–liquid interface. The most important driving forces for biomolecule adsorption on a surface are electrostatic interactions, van-der-Waals interactions, hydrogen bonds, and hydrophobic interactions. Below, we first present the physicochemical conditions that influence biomolecule adsorption and then the parameters that are used to describe and characterize biomolecule adsorption at surfaces.

### A. Physicochemical properties of the biomolecule, liquid medium, and surface

There are three key parameters contributing to the interactions between a biomolecule and a surface.

#### *1. Physicochemical properties of the biomolecule (protein, polymeric chain, lipids, etc.)*

Regarding proteins, their size depends on the number of amino acid and can vary from a few nanometers to tens of nanometers. Their composition in amino acids influences the intramolecular forces that define their conformation, their isoelectric point (pH at which their global charge is neutral), and their global shape, which can be symmetric for globular proteins (such as albumin or insulin) or asymmetric for elongated and Y-shaped proteins, such as fibronectin and IgG.[17]

The diffusion coefficient (D, in $\mu m^2/s$) depends on the size and shape of the proteins. It defines the time needed for the proteins to reach the surface. In complex mixtures of proteins, protein adsorption is a competitive process, in which adsorbed proteins can subsequently be replaced by others, depending on their respective binding strength. This phenomenon, known as the Vroman effect,[18] describes the replacement of a fast adsorbing protein with low surface affinity by a slow adsorbing protein with a higher surface affinity. The adsorption of biomolecules can be random or directed at a specific position, depending on the intermolecular interactions between the biomolecules and the interactions between the biomolecules and the underlying surfaces [Fig. 1(a)]. The orientation of adsorbed molecules can be in plane (e.g., x, y directions) or out of plane (x, y, z directions) [Fig. 1(b)] in case the biomolecules are anisotropic and forming long-range aggregates in the direction perpendicular to the sensor surface. The interactions between the

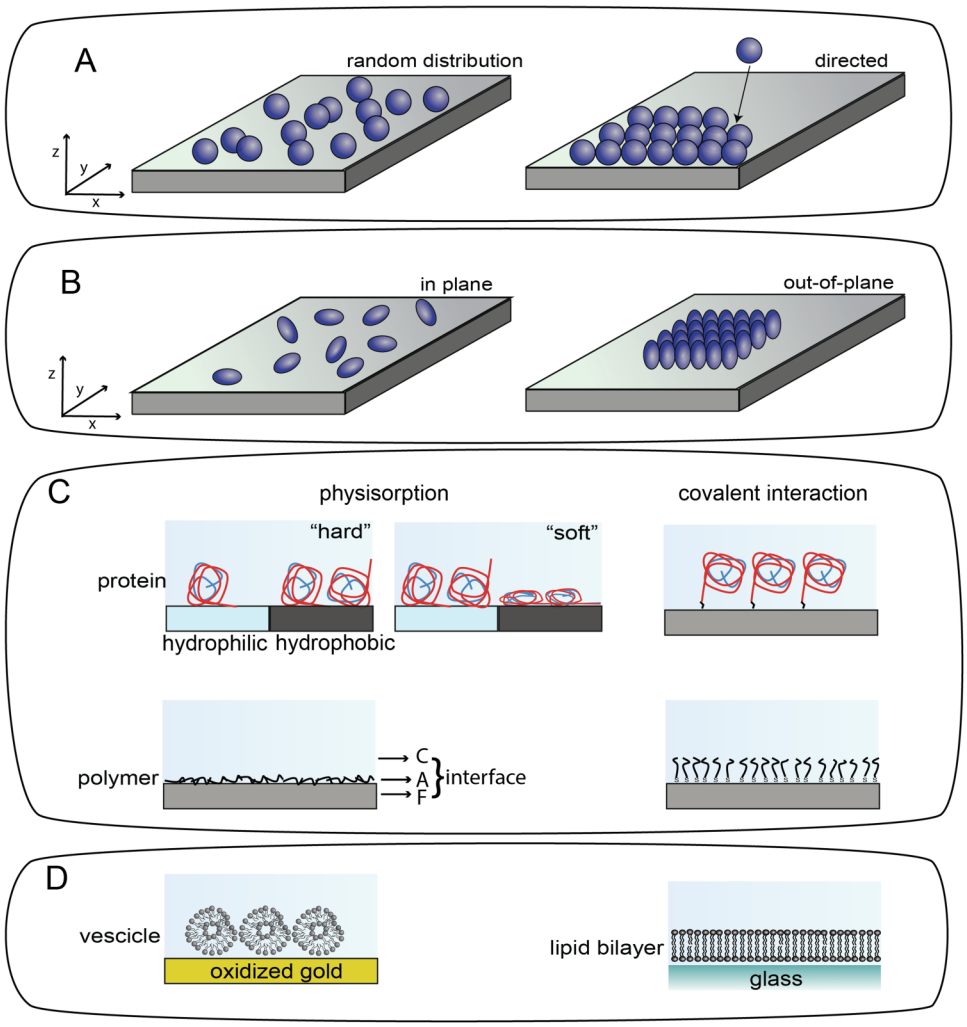


FIG. 1. Schematic representation of molecular adsorption on surfaces and of important parameters to consider. (a) Schematic representation of a random or directed adsorption of molecules to a specific position on the surface; directed here means that molecular interactions between the biomolecules guide their spatial organization at the surface of the sensor material. (b) Schematic representation of the adsorption of anisotropic biomolecules either on the surface (x, y) plane or out of plane (x, y, z). (c) Proteins can be physisorbed on hydrophilic and/or hydrophobic surfaces or grafted via site-specific covalent functionalization. Hard proteins only marginally change conformation when physisorbed on surfaces; on the contrary, soft proteins can change their conformation when physisorbed on hydrophobic surfaces. Polymers can also be grafted and oriented on a surface via covalent interaction or randomly physisorbed. In the following, we will use the following nomenclature: F for the materials sensing substrate, A for the adsorbed layer of biomolecules whatever their type (proteins, polymers, lipids, etc.), and C for the cover medium (i.e., liquid medium above the adsorbed layer, which can be a buffered solution or any other type of solution). (d) Lipid vesicle adsorption on a surface is surface-specific; they remain intact on oxidized gold, whereas on glass they fuse forming a planar supported lipid bilayer.

biomolecules and the surface, the intermolecular interactions between the biomolecules themselves, as well as the anisotropy of the biomolecules (shape and the presence of different molecular domains) are factors contributing to the packing density, orientation, and adsorbed amount of the biomolecules as well as, in the case of bioactive proteins, their biological activity. Notably, with increasing surface coverage, protein–protein interactions can change surface adsorption kinetics, leading to positive or negative cooperativity.[6,14]

Given the structural complexity of proteins, it is very difficult to find simple ways of predicting their adsorption behavior at interfaces. An attempt to classify proteins into "hard" and "soft" ones, describing their propensity for structural modification upon surface binding, was made by Arai and Norde.[19] "Hard" proteins tend to adsorb on surfaces undergoing none or only small conformational changes, whereas more extensive structural reorientations accompany surface adsorption of "soft" proteins. "Hard" proteins tend to adsorb preferentially on hydrophobic surfaces and their adsorption is largely dominated by hydrophobic and electrostatic interactions [Fig. 1(c)]. In contrast, because of their low internal stability, "soft" proteins tend to adsorb well on both hydrophobic and hydrophilic surfaces, compensating the loss of hydration of the protein and the surface and electrostatic interactions by a gain in folding entropy.

Polymeric chains have a certain length and charge density. Polymers can be grafted and orientated on a surface

TABLE I. Comparison of the different surface-sensitive techniques used to characterize the adsorption of biomolecules on a surface: their physical principle, deduced parameters, sensing depth ($d_P$), type of surface, drawbacks, advantages, and ease of use are compared. $d_A$: film thickness (nm); $d_P$: penetration depth; $n_A$: refractive index; Γ: adsorbed mass in mass per surface area (ng/cm$^2$ or $\mu$g/cm$^2$). SPR(i): surface plasmon resonance (imaging); OWLS: optical waveguide lightmode spectroscopy; DPI: dual polarization interferometry; ATR-FTIR: attenuated total reflection Fourier transform infrared spectroscopy; SE: spectroscopic ellipsometry; QCM-D: quartz crystal microbalance with dissipation monitoring; AFM: atomic force microscopy.

| Method | Physical signal | Deduced parameters | Sensitivity Γ ($d_A$) | Sensing depth ($d_P$) | Type of surface | Drawbacks | Advantages | Ease of use | References |
|---|---|---|---|---|---|---|---|---|---|
| ELISA | Colorimetry, fluorescence, and luminescence | Γ = (endpoint) | fM range | | Multiwell plate (plastic); beads (e.g., PS) | Necessity for specific antibody<br>Diffusion limited<br>Long time (h) | High specificity and sensitivity<br>Automatization<br>High throughput | ++++ | 49 |
| SPR | *Evanescent wave*<br>Variation of resonance angle | Γ = (time) kinetic interaction parameters<br>Affinity concentration | 1 pg/mm$^2$<br>Few tens of nm | $d_P$ ~20 nm[a] | Functionalizable<br>Au-coated chips | Relatively small sensing depth<br>Cost of sensors<br>Limited parallelism | Very high sensitivity<br>Real time analysis | ++ | 59 |
| SPRi | *Evanescent wave*<br>Fixed angle; variation of reflected light | Γ = (time); kinetic interaction parameters; affinity | 1 pg/mm$^2$ | 20 nm[a] | Functionalizable<br>Au-coated prism | Relatively small sensing depth and high cost of sensors | Very high sensitivity<br>Real time analysis<br>Parallel analysis of several hundred spots | ++ | 59 |
| OWLS | *Evanescent wave*<br>Transverse electric and magnetic modes excited in the waveguide | $n_A$, $d_A$,<br>Γ (time) | <1 ng/cm$^2$<br>0.1 nm | $d_P$ ~150 nm[b]<br>$d_A$ max ~400 nm[b] | $SiO_2$-$TiO_2$ sol gel waveguide layer | One provider (MicroVacuum) one measurement at a time<br>$n_A$ and $d_A$ intrinsically linked (Γ being the invariant) | *In situ* adsorption/desorption kinetics in real time<br>High sensitivity (<1 ng/cm$^2$, 0.1 nm for dA)<br>Now available at high throughput in microplates | + | 72,131 |
| DPI | *Evanescent wave*<br>Phase shift of TE and TM waves<br>Analysis of interference pattern | $n_A$, $d_A$, density $\rho_A$<br>Γ = (time) | <1 ng/cm$^2$<br>0.1 Å<br>$n_A$ ~$10^{-4}$ | Unknown | Si oxynitride | Only relative parameters can be obtained<br>Sensitive to wavelength instabilities<br>Sensitive to mechanical vibrations<br>$n_A$ and $d_A$ intrinsically linked (Γ being the invariant) | Very high sensitivity (0.001 for nA; 0.01 nm for dA)<br>Interaction with the sample over several mm or cm | +++ | 81,82 |
| ATR-FTIR | *Evanescent wave*<br>IR light transmitted through a high *n* guiding crystal (absorbance) | Secondary structure of proteins<br>IR peaks of chemical groups | 100 ng/cm$^2$<br>~1 nm | $d_P \approx$ 900–1500 nm | Crystal of:<br>ZnSe<br>Si<br>Ge | Need to work in $D_2O$<br>Not highly sensitive<br>Large volume required (mL)<br>Peaks need to be deconvoluted | Sensing over long distance<br>Specificity of IR bands<br>Hydration state (H-bonds) | + | 95,132 |
| SE | Change in light phase or intensity:<br>Ψ, Δ of reflected light | $n_A$, $d_A$ | <1 nm | From 1 nm (UV) to >1 μm (IR) | Au or $SiO_2$ | Complicated modeling to estimate $n_A$ and $d_A$ based on Ψ and Δ. One measurement at a time | Measure of optical masses in real time with high sensitivity. No limitation in refractive index and film density<br>High penetration depth | + | 99 |

TABLE I. (*Continued.*)

| Method | Physical signal | Deduced parameters | Sensitivity $\Gamma$ ($d_A$) | Sensing depth ($d_P$) | Type of surface | Drawbacks | Advantages | Ease of use | References |
|---|---|---|---|---|---|---|---|---|---|
| QCM-D | Change in frequency shift of quartz crystal ($\Delta f$) and of dissipation ($\Delta D$) | Hydrated mass, Viscoelastic modulus | 1 ng/cm$^2$ 0.1 nm | ~1 $\mu$m | Au, $SiO_2$, $TiO_2$, Zn, and Mb | Measurement of the molecular mass adsorption always coupled with the solvent. Energy dissipation impacts mass calculation | *In situ* adsorption/desorption kinetics in real time Viscoelastic properties Four measurements in parallel | +++ 4 parallel | 108,112 |
| AFM | Tip–sample forces | x-y-z positions, Young's modulus, chemical mapping | ~0.1 nm | Up to 100 | All surfaces | Very difficult to image very soft films The resolution depends on the tip curve-radius Highly sensitive to working environment Not high throughput technique | Imaging biological molecule in their physiological environment. x-y-z information on the sample distribution on the surface | + | 117 |

[a]Reference 63.
[b]Reference 75.

via covalent interactions or physisorbed randomly [Fig. 1(c)]. Supported lipid membranes are important to study the properties and functions of membrane-bound proteins. In particular, the goal of synthetic biology is the assembly of biomimetic cell-like structures, which combine multiple biological components in synthetic lipid vesicles. It is well known that the fusion of lipid vesicles forming 2D supported lipid bilayers depends on the substrate composition.[20] They remain as compact vesicles on oxidized gold substrates and they fuse at a critical surface concentration on $S_iO_2$ [Fig. 1(d)]. More recently, a one-step procedure, called the solvent-assisted lipid bilayer formation method, has been developed in order to form supported lipid bilayers which do not require vesicles and is compatible with different surfaces, not only $S_iO_2$.[21]

## 2. Liquid medium

The pH of the solution influences the net charge of proteins and of polymeric chains that contain charged functional groups (such as carboxylic acid, sulfate, phosphate for the negative ones, and ammonium for the positive ones). The ionic strength of the solution defines the distance (Debye length) at which electrostatic interactions are effective in an electrolyte solution. It thus influences attractive or repulsive interactions between charged biomolecules and surfaces, affecting the molecular interactions and their adsorption kinetics. The type of buffer [phosphate buffer (PBS), 2-(N-morpholino)ethanesulfonic acid, …] and ions present in solution (monovalent such as $K^+Cl^-$ or $Na^+Cl^-$ or divalent such as $Ca^{2+}$ and $Mg^{2+}$) also impact on molecular interactions, since the ions have affinities with functional groups, as is the case of phosphate groups for calcium ions.[22]

## 3. Surface properties

The properties of the surface such as the type of functional group, charge, and hydrophobicity can all influence biomolecule adsorption. For adsorption studies, chemically well-defined surfaces are usually obtained by surface functionalization. This is commonly achieved using self-assembled monolayers[23] or polymer brushes[24] made of polyethylene oxide or PEG.[25] The polymers can be deposited by physical adsorption (physisorption) using dip- or spin-coating or grafted by various strategies[26] [Fig. 1(b)]. Polymers may be used to minimize protein adsorption through steric effects and excluded volume effects.[27] Usually, proteins tend to adsorb more strongly on hydrophobic than hydrophilic surfaces, on charged than on uncharged surfaces. Finally, model lipid membranes (supported lipid bilayers) can also be used to mimic protein interactions with the plasma membrane present in cells.[28]

The topography of the surface, especially its roughness at the nanometer and even micrometer scale, may strongly influence protein adsorption and conformation.[29,30]

## B. Parameters used to characterize biomolecule adsorption

### 1. Surface-adsorbed amount

An important parameter that is measured by several techniques (see below) is the adsorbed mass, expressed in mass per unit area ($\Gamma$ usually in ng/cm$^2$ or $\mu$g/cm$^2$). The results vary with the experimental setups (variable surface area and chemistry), the timescales, and the sensitivities of the respective techniques, and it remains challenging to compare different studies. For proteins, there are different models describing their adsorption/desorption behavior at interfaces,[31] the most widely known being the Langmuir model and the random sequential adsorption model. However, these models have two main limitations:[31] first, the equilibrium hypothesis does not apply as desorption experiments generally lead to a residual, irreversibly bound protein fraction and desorbed proteins can potentially readsorb at the surface. Second, these models do not account for interactions between surface-adsorbed molecules such as rearrangements with increasing surface coverage. Therefore, care should be taken to consider an accurate description corresponding to the observed adsorption and desorption phenomena. Adsorption may be ideally recorded in real time (time resolution <1 min) in order to follow the adsorption kinetics. It may be sigmoidal, indicating that some cooperativity between the biomolecules occurs during adsorption.[32] This cooperativity may be due to intermolecular interactions leading to aggregate formation.[33] In general, at low surface coverage, Langmuir-type adsorption takes place which is subsequently replaced by a cooperative adsorption at higher surface coverage.[32] Typical adsorbed protein amounts are in the order of hundreds of ng/cm$^2$.[16] In most cases, the irreversibly adsorbed amount corresponds to a protein monolayer although stably adsorbed protein multilayers have also been documented.[34] Very often repulsion between adjacent adsorbed proteins entails monolayer formation. Multilayers are typically found in conditions that reduce protein–protein repulsion and promote aggregation.

### 2. Conformational change upon adsorption

In solution, biomolecules are surrounded by a shell of water molecules that are associated with it and contribute to its stable conformation. Upon surface adsorption, the biomolecules may undergo rapid conformational changes to increase the surface contact area and stabilize the adsorption by a maximization of interaction forces with the surface (footprint).[14] For instance, on a hydrophobic surface, protein adsorption is accompanied by an entropy gain resulting from the release of surface-adsorbed water molecules and ions and turning previously buried hydrophobic side chains toward the surface.[14] Such surface-induced reorientations result in partial unfolding of the adsorbed proteins so that a stabilization at the interface can be achieved. The protein–surface interactions and the entropy gain from conformational relaxation contribute to a new free energy minimum of the adsorbed state of the protein. In general, structural changes in adsorbed proteins are more prominent on hydrophobic surfaces than on hydrophilic ones and vary according to the inherent stability of the protein. The consequence of this relaxation (unfolding and/or reorientation) is the establishment of an often irreversibly bound protein fraction, at least within the timeframe of most experimental approaches.

Beyond biomolecule–surface interactions, protein–protein interactions also influence the final state of the adsorbed species.[31] Lateral interactions via electrostatic forces gain importance as adsorption proceeds. These lateral interactions influence the conformational state of the adsorbed biomolecule so that the balance between biomolecule/biomolecule and biomolecule/surface interactions changes which may even lead to desorption.

### 3. Aggregation state

Surface adsorption can induce the formation of intermolecular protein aggregates, which are defined as irreversible complexes between two or more protein monomers presenting regions of extended, strong, noncovalent interactions between the monomers. Such surface-bound aggregates can be formed either by lateral diffusion or by direct binding onto preadsorbed proteins.[35] The latter is the case, for instance, of hydrophobic surface-induced amyloid fibrillation of insulin.[36,37] In this case, adsorbed proteins form clusters (nuclei) on the surface which, at a critical size, induce the growth of surface-bound amyloid fibers. Upon agitation, such protein aggregates can be released in solution which can trigger further surface aggregation and sometimes aggregate growth in solution. In the case of therapeutic proteins, surface-induced aggregate formation and their release into solution is considered as an important risk factor. The understanding of the underlying mechanisms, the design of more stable molecular variants, and the control of the processes involved are all subject to intensive research efforts.[38]

### 4. Reversibility of adsorption

Protein surface adsorption can be considered reversible or irreversible according to three different conditions: reversible upon dilution, reversible upon changing the physicochemical conditions (pH, ionic concentration, etc.), and reversible upon exchange with other proteins (for example, "Vroman effect"). Adsorption to hydrophobic surfaces is usually irreversible with respect to dilution, whereas adsorption on hydrophilic surfaces, which is dominated by electrostatic interactions, is subject to reversibility upon pH or ionic strength changes in the solution.[39] Homomolecular exchange at the surface has been documented for several proteins and surfaces,[40] whereas other proteins do not undergo such exchanges[41] or change their behavior depending on the surface.[42] In the context of therapeutic proteins, an important question is whether the protein released from the surface retains its conformational change or not.

## III. EXPERIMENTAL TECHNIQUES TO CHARACTERIZE BIOMOLECULE ADSORPTION AT SURFACES

Below we describe the experimental techniques to characterize the adsorption of biomolecules at the solid–liquid interface and for each, present their physical principle and measured parameters. We decided not to present techniques that require a very large amount of sample and need specific working conditions (e. g. deuteration), such as neutron reflectometry[43,44] or that are done in dry state, such as time of flight secondary ion mass spectrometry.[45] We also decided to focus solely on label-free techniques and will not present all the fluorescence-based techniques, which are powerful but require the molecule to be labeled with a fluorophore. After a literature search, we decided to classify them into different categories: (i) enzyme-linked immunosorbent assay (ELISA) was set apart, since it is the most widely used test in biology, already applied in medicine and is thus considered as a reference, (ii) optical-based techniques that rely on evanescent waves. In this category, we find surface plasmon resonance (SPR), optical waveguide lightmode spectroscopy (OWLS), dual polarization interferometry (DPI), and Fourier transform infrared spectroscopy in attenuated total reflection mode (ATR-FTIR). (iii) Acoustic techniques such as quartz crystal balance with dissipation monitoring (QCM-D) and other optical techniques such as spectroscopic ellipsometry (SE) that rely on reflected light. Finally, atomic force microscopy (AFM) is used for surface imaging at high resolution.

We will not describe the optical equations that describe the propagation of electromagnetic waves, which are at the basis of all equations used in the optical-based sensing techniques. The reader is advised to read text books to understand the underlying principal of electromagnetism.[46]

Several major parameters can be deduced:

(i) Static parameters, including the layer thickness ($d_A$, in nm), its refractive index $n_A$, and the adsorbed mass ($\Gamma$ in ng/cm$^2$). $\Gamma$ is usually determined by approximation using the well-known De Feijter formula,[47] considering that it is proportional to $n_A$ and film thickness $d_A$.

$$\Gamma = \frac{(n_A - n_C) \times d_A}{(dn/dc)} (\text{in ng/cm}^2), \quad (1)$$

where $n_C$ is the refractive index of the suspending medium and $dn/dc$ is the increment of the protein refractive index as a function of protein concentration. This is normally determined with a refractometer and is usually considered to be a fixed value of 0.188 mL/g, but is in fact following a distribution.[48]

(ii) Kinetic parameters such as $k_{on}$ and $k_{off}$ may also be estimated.

(iii) Secondary structure in proteins (percentage of α-helices and β-sheets).

For each technique, we provide information on the physical principle, the measured parameters, and their advantages and drawbacks (Table I).

### A. ELISA

The ELISA is a technique that uses a solid support (multiwell plates, beads) for the molecular quantification of immune-complexes via signal amplification through an enzymatic reaction readout.[49] In its most common format, the antigen to be quantified is sandwiched between a capture antibody, linked to a surface, and a detection antibody, recombinantly fused with horse reddish peroxidase or alkaline phosphatase. This format allows for high specificity and sensitivity (typically in the fM range), two parameters that are key in diagnosis, in which ELISA tests represent a gold standard. Classically, the ELISA has been developed in different variants: direct, indirect, sandwich, or competitive formats are described, depending on the sequential buildup of the immune-complex to be tested. The enzymatic reaction generates usually a colored product which is quantifiable via spectrophotometry using appropriate calibration curves. Different readouts using a fluorescent, electrochemical, or luminescent signal are also used. The ELISA protocol is based on sequential incubation steps, generating the immune-complex to be detected on the solid support and eliminating nonincorporated molecules with intermediate washing steps. As the immune-complex is formed on a surface, nonspecific surface binding has to be minimized by efficient blocking using BSA or milk proteins. The reaction rates are limited by diffusion of the biomolecules, generating therefore relatively long incubation times (h). Since the 50 years of its existence, the classical ELISA test has seen its protocol adapted to high throughput automatization (1000 tests/h) using highly parallelizable systems, minimizing volume, and therefore, reducing time.[50] The introduction of micrometric beads as a solid support allowed the immune reactions to take place in the suspension, thus decreasing the diffusion time while increasing the reaction surface dramatically. Using magnetic beads that can be trapped in a magnetic field, facilitates washing steps, contributing to time and cost minimization.[51] Recent developments using mixtures of beads coated with different capture antibodies opened the way for highly parallel multianalyte profiling. Also, fluorescence readouts combined with sorting of beads carrying the immune-complexes into single molecule arrays by lab on disc microfluidics have allowed to push the detection limits to 0.01 pg/mL.[52]

### B. Surface plasmon resonance

Among optical biosensing techniques, SPR is one of the most prominent with applications in many fields and a particularly high impact in pharmaceutical sciences.[53] Since its commercialization in the 1990s, SPR has been developed in different formats rising to the challenging requirements for high sensitivity and high throughput.[54] A recent review by Mauriz *et al.*[55] covers SPR-based assays in great detail.

SPR measures variations of the refractive index in close proximity (up to ~300 nm) of a sensing surface [Fig. 2(a)]. Such refractive index changes are brought about with mass changes in the sensing layer that occur upon molecular binding events. The sensor is generally made of a thin gold

layer (~50 nm) deposited at the surface of a glass prism. Polarized light is shone at variable angles and in conditions of total internal reflection through the glass prism onto the gold layer. Plasmon resonance occurs when the electrons of the gold atoms adsorb energy from the photons provided by the illumination at the resonance angle. An evanescent wave is then propagated at the gold/solution interface. The measurement of the intensity of the reflected light allows the resonance angle to be determined. The adsorption of biomolecules changes the refractive index ($n_A$) at the gold/solution interface and the layer thickness ($d_A$), which is related to the change in resonance angle θ. The underlying equations are complex and cannot be given in a simplified manner.[56] Thus, we decide not to provide details of these equations. Instead, we selected a tutorial about SPR (Ref. 57) that provides a relationship between θ and the refractive index of the absorbed layer [Eq. (2)].

$$\theta = \sin^{-1}\frac{1}{n_F}\sqrt{\frac{n_A^2 n_g^2}{n_A^2 + n_{g_1}^2}}, \tag{2}$$

where $n_F$ is the high refractive index below the gold layer, $n_G$ is the refractive index of the gold, and $n_A$ is that of the adsorbed layer. As a first approximation, the change in θ is linearly related to $n_A$.[57] The signal, which corresponds to the measured shift in this resonance angle, is expressed as responds units (RU; 1 RU = $10^{-4}$ degrees). SPR is sensitive to the adsorbed mass, the detection limit being ~0.1 ng/cm$^2$.[58] Besides the ability of the sensor to detect the adsorbing biomolecules, i.e., the intensity of physically detected biomolecules, also depends on the molecular weight of the adsorbing biomolecules: if these are of very small molecular weight (below 100 g/mol), then it will be very difficult to detect them at the early stage of their adsorption, even if they are at high volumic concentration in solution. This is due to the fact that the number of biomolecules (directly related to the mass) effectively adsorbed may be below the detection limit of the sensor. This is particularly true at the beginning of the adsorption, meaning that it may not be possible to quantify the kinetic parameters ($k_{on}$) but solely to follow the kinetics once the adsorbed mass is above the detection limit of the biosensor.

SPR allows real time measurements of molecular binding events and is often used for the determination of association and dissociation rates, affinity constants, binding typology, and concentration of molecular reactants. Beyond interaction analyses, SPR has also been used to study conformational changes to detect mutations, to identify biomarkers, to perform high throughput screening for drug discovery and development, and to study cell responses.[59]

In general, one interacting species (ligand) is immobilized on the sensor surface while the second one (analyte) is flown over the surface in a controlled flow, operated by a microfluidic system. The binding of the ligand can be covalent using $NH_2$, SH, or COOH coupling chemistries or noncovalent, relying on affinity interactions (e.g., biotin-streptavidin, protein G-antibody, $Ni^{2+}$-His tag, sequence-specific DNA-directed immobilization).[59] According to the chosen immobilization strategy, the orientation of the ligand can be random or directional, which can impact the sensitivity of the studied interaction. Nonspecific adsorption on the sensor surface is one of the major drawbacks in SPR experiments, as well as with the other experimental techniques presented below, but it can be minimized using commercially available sensors with inert surface functionalization such as hydrophilic, protein-repellent carboxymethylated dextran layers. Block copolymers of polyethyleneglycol (PEG) and methyl methacrylate may also be used.[60,61] Parallel and high throughput analyses are limited in conventional SPR setups by the number of flow channels. In order to do high throughput analysis and reduce time and cost, SPR has been developed in the imaging mode (SPRi). In this mode, the technique is operated at a fixed illumination angle, and a charge-coupled device camera continuously images the interaction surface and records variations of the reflected light over the entire surface, at each position of arrays of hundreds to thousands of different immobilized ligands.

The adsorbed layer can be probed until a defined thickness, limited by the penetration depth of the SPR signal. This is typically in the 100–250 nm range for wavelengths in the visible spectrum. Figure 2(a′) shows an example of a study probing the linearity of the signal with respect to the amount of adsorbed polyelectrolytes. On an anchoring layer of adsorbed polyethyleneimine, the buildup of a polyelectrolyte film using alternate layers of polystyrene sulfonate (negatively charged) and polyallylaminehydrochloride (positively charged) was recorded. The thickness of these films had been previously shown, using QCM-D and waveguide spectroscopy, to increase linearly by 3–5 nm per layer.[62] Using the rapidly decreasing amplitude of the SPRi signal for each layer adsorption, the penetration distance of the SPRi signal could be estimated to roughly 20 nm in this experiment.[63]

In the SPRi mode, the kinetics of protein or polyelectrolyte adsorption can be recorded on customized chemical functionalizations applied to the gold layer. A dually functionalized prism with a hydrophilic (SH-PEG) and a hydrophobic (SH-C16) side was thus used to study the preferential adsorption of human insulin on hydrophobic surfaces [Fig. 2(a″)]. The SPR signal recorded on the hydrophilic surface was attributed solely to refractive index changes of the protein solution compared to the buffer, since it was shown using other techniques that the protein did not adsorb on hydrophilic surfaces. The SPR signal recorded on the hydrophobic surface documents a fast and important adsorption of insulin followed by a slower linearly increasing adsorption. The dissociation of insulin from the hydrophobic surface is not fully reversible and documents that a very strongly adsorbed protein layer remains surface-bound.[63]

Sensitivity and resolution improvements have been obtained with the more recent development of local SPR (LSPR) in which the sensing is localized on metallic nanoparticles (smaller than the wavelength of incident light), amplifying the

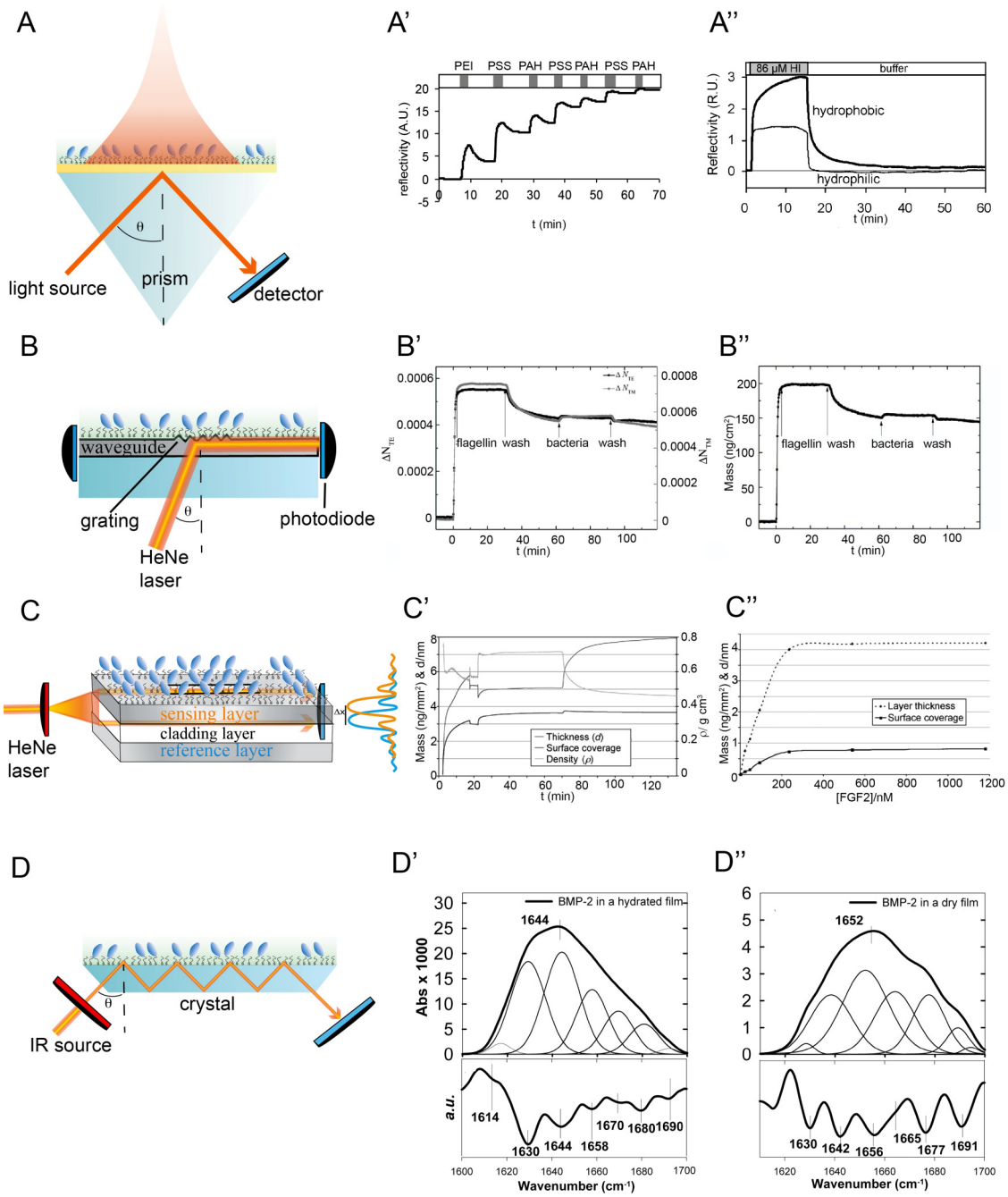


FIG. 2. (a) SPR general principle. (a′) SPRi recording of polyelectrolyte layer-by-layer film built on a gold surface. (a″) Human insulin association and dissociation kinetics on hydrophobic/hydrophilic surfaces measured by SPRi. Adapted with permission from Nault *et al.*, Acta Biomater. **9**, 5070 (2013). Copyright 2013, Elsevier. (b) OWLS general principle. (b′) OWLS measurement of the effective refractive indices ($\Delta N_{TE}$ and $\Delta N_{TM}$) during protein and bacteria adsorption and desorption on a hydrophobic surface. (b″) Adsorbed mass calculated from the recorded effective refractive index shifts during the *in situ* OWLS measurement. Arrows indicate the times when the sample solutions reach the sensing area. Reproduced with permission from Kovacs *et al.*, Sens. Actuators B: Chem. **257**, 839 (2018). Copyright 2018, Elsevier. (c) DPI schematic representation. (c′) Changes in surface coverage and dimensions of a linker used to bind heparin on gold. The linker was added at ca. t = 3 min, and following PBS washing, the heparin was added at 21 min. After 70 min, the surface was washed with PBS. (c″) The changes in thickness and surface coverage were measured for FGF-2 binding to a surface previously immobilized with heparin dp10. Reproduced with permission from Popplewell *et al.*, Chembiochem **10**, 1218 (2009). Copyright 2009, Wiley. (d) ATR-FTIR general principle. [(d′)–(d″)] FTIR spectra and second derivative of BMP-2 trapped in (d′) hydrated polyelectrolyte (poly-L-(lysine)/hyaluronic acid) films and (d″) dried films (black: experimental spectrum; gray: fitted spectrum). Adapted with permission from Gilde *et al.*, Biomacromolecules **13**, 3620 (2012). Copyright 2012, American Chemical Society.

signal to the pM range.[64] Different formats of LSPR are discussed in recent reviews, opening the way for the integration of SPR in point of care devices.[65,66] Microscope-objective type SPR designs are also developed, allowing pixel-by-pixel tracking of the reflectivity in the SPR images to overcome the spatial resolution limited by the numerical aperture of the prisms.[67] Finally, efforts are made to integrate SPR with other relevant characterization techniques like mass spectrometry, for

example,[68] or to incorporate it in optical fibers for miniaturized sensing probes.[69]

### C. Optical waveguide lightmode spectroscopy

OWLS is a sensitive, label-free, optical waveguide biosensor [Fig. 2(b)]. It is constituted of a grating embossed in a high refractive index layer (F) made of $TiO_2/SiO_2$ (refractive index $n_F \approx 1.77$, thickness $d_F \approx 180$ nm). A helium–neon laser beam ($\lambda = 632.8$ nm) propagates through the glass substrate, S (refractive index nS), and arrives on the grating that is embossed within the film (F) with an incidence angle θ. The effective refractive index (N) depends on the wavelength and on the mode in which the light propagates [transverse electric (TE) or transverse magnetic (TM)]. It is named *NTE* for the transverse electric mode and *NTM* for the transverse magnetic mode, which are guided in the film F by total internal reflection. There is an evanescent wave at the film/adsorbed biomolecule layer/suspending cover medium (F/A/C) and film/glass substrate (F/S) interfaces.

$$N = \sin\theta + \frac{l\lambda}{\Lambda}, \tag{3}$$

where l is the diffraction order (equal to 1) and Λ is the grating constant.

The incoupled guided modes propagate in the waveguiding film (F), and the intensity of the light is monitored via two photodiodes. The effective refractive indices of the guided modes *NTE* and *NTM* are highly sensitive to changes of the optical parameters of the adsorbed layer (refractive index $n_A$ and thickness $d_A$) that is adsorbing in the suspending medium of refractive index $n_C$. The mode equations lead to the corresponding expression for the phase shift Φ:[72]

$$\Phi = 2k_{z,F}d_F + \Phi_{F,S} + \Phi_{F,A,C} = 2\pi m, \tag{4}$$

$\Phi_{F,S}$ being the phase shift at the F/S interface and $\Phi_{F,A,C}$ being the phase shift at the F/A/C interface:

$$\phi_{F,A,C} = \phi_{F,C} + 2k_0 f \frac{n_A^2 - n_C^2}{n_F^2 - n_C^2} \times \left[\frac{(N/n_C)^2 + (N/n_A)^2 - 1}{(N/n_C)^2 + (N/n_F)^2 - 1}\right]^{\rho} d_A + O(d_A^2), \tag{5}$$

with $\rho = 0$ for the TE mode and $\rho = 1$ for the TM mode.

The waveguide parameters, $n_F$ and $d_F$, are initially derived from the *NTE* and *NTM* equilibrium values when the buffer alone is in contact with the film F and $d_A = 0$.[72] The modeling generally assumes homogeneous isotropic layers and that the adsorbed layer is very thin in comparison to the wavelength of the light ($d_A \ll \lambda$). When no assumption is made on $d_A$, then the equations are more complex and $d_A$ values deduced from the fit differ greatly, especially for values >40 nm.[73]

The theoretical values of the penetration depth $d_P$ of the evanescent waves for the two modes can be calculated.[73] They are in the order of 170 and 225 nm, respectively, for NTE and NTM.[73] The detection limit of the adsorbed amount is ~1 ng/cm$^2$. Typical values for $n_A$ range from 1.36 to 1.5. $n_A$ is close to 1.36 when the layers are ultrathin, hydrated, and swollen as is the case for dextran[74] or hyaluronan layers.[75]

OWLS has been widely used to study *in situ* protein adsorption onto surfaces, covalent grafting of biomolecules, such as ethylene glycol dendrons,[76] and growth of layer-by-layer films.[73,77] Indeed, linearly growing LbL films were used to assess the experimentally measured limit of biomolecule sensing, which was found to be in the order of 400 nm.[73] This value is about twofold the theoretical value for the penetration depth. The nature of the adsorption (reversible/irreversible) can also be assessed by comparing the signal after washing to the initial baseline value.[74]

An analysis was developed in order to take into account a possible anisotropy of the adsorbed layer leading to birefringence.[78] In this case, $n_A$ consists of ordinary ($n_O$) and extraordinary refractive indices ($n_E$). It was applied to the adsorption of flagellin layers [Figs. 2(b′) and 2(b″)].[78] Changes in the refractive index provide information on the structure (orientation) of the layers. It was applied to study the grafting of carboxymethylated dextran on aminosylated or epoxysylated surfaces.[74]

Recently, a planar optical waveguide made of a biocompatible material, $Nb_2O_5$, was designed at the bottom of commercially available microplates (Epic) to do high throughput characterization of the adsorption of green tea catechols and subsequent cell adhesion.[79] New experimental developments also focus on the integration of a grating coupled interferometer and spectroscopic ellipsometer into one single tool.[80]

### D. Dual polarization interferometry

DPI is an optical waveguide interferometer developed by Freeman *et al.*[81–84] [Fig. 2(c)]. It is composed of three layers: a reference layer, a cladding layer, and a sensing layer located on top where the biomolecule will be adsorbed. Two parallel openings are etched into the upper cladding layer; therefore, two-channel measurements can be performed in a biosensor experiment.

The HeNe laser light ($\lambda = 632.8$ nm) illuminates the end face of the two stacked planar waveguides and a small fraction of it is coupled into the two waveguides. The two polarization modes (in plane, parallel TE and out of plane, transverse TM, respectively) are alternatively sent by switching the polarization every 2 ms, which allows quasisimultaneous measurements of the adsorption process. Classical Young's fringes are obtained in the far-field diffraction plane and recorded on a CCD camera as a two-dimensional interference pattern.[81] A Fourier transformation enables the phase shift Φ of TE and TM modes to be calculated in real time during the adsorption of the layers [Eq. (6) taken from Ref. 84]:

$$\Delta N_{TX_0}(t) = \left(\frac{\lambda}{L\Lambda}\right)\Delta x(t) = \left(\frac{\lambda}{2\pi L}\right)\Delta\phi(t), \tag{6}$$

where $TX_0$ denotes $TE_0$ or $TM_0$ and Δx is the spatial shift of the interference fringes.

Λ is the spatial period of the fringes and L is the interaction length.

For each polarization mode TE and TM, the range of possible combinations of layer thickness and refractive index values is calculated. There will only be one unique combination that satisfies the range of solutions found for TE and TM.

Besides the phase shift, the fringe contrast (difference between the peak maximum and peak minimum) enables to obtain information from the adsorption or scattering processes that occur at the interface.

When the adsorbed layer is anisotropic, it may be characterized by birefringence (see above for OWLS). In practice, it is assumed that $N_{TE} = n_O$ and $N_{TM} \approx n_E$ and that:

$$n_{anisotropy} = n_E - n_O. \tag{7}$$

DPI thus allows the anisotropy of the layer to be measured in real time.

Researchers usually calculate the density of the layer ($\rho_A$):[85]

$$\rho_A = \rho_P \frac{n_A - n_C}{n_P - n_C} = (n_A - n_C) \times \frac{dn}{dc}, \tag{8}$$

where $\rho_P$ is the volumic concentration of protein within the adsorbed layer (g/mL) and $n_P$ is the protein index. In order to calculate $\rho_A$, the absolute properties of the proteins ($n_P$, $\rho_P$) need to be determined from solution measurements with a refractometer.

To note, $\Gamma = \rho_A \times d_A$ [see Eq. (1) above].

During the past years, DPI has been increasingly used[86] for studying carbohydrate/protein interactions,[85] the adsorption of various biomolecules, such as DNA, proteins, lipids, and membranes,[87] and polyelectrolytes, including layer-by-layer deposition. In particular, it enables to study the adsorption kinetics in real time with a resolution of seconds. Changes in conformation of proteins during their adsorption and aggregation can also be followed.[88,89] DPI has been used to study the binding of protein to glycosaminoglycans (GAGs) as chondroitin sulfate, keratin sulfate, and heparin.[71] The reducing end of GAGs has been grafted onto a hydrazide-functionalized surface and their surface coverage, the thickness of the layer, and its density were followed with DPI [Fig. 2(c′)]. The binding of fibroblast growth factor 2 (FGF2) to grafted heparin (deca) oligosaccharides has been characterized. With DPI, the authors proved that FGF2 binds on top of the heparin film, which increased in thickness by 4 nm [Fig. 2(c″)]. The binding affinity has also been measured proving the multiple use of this technique not only to analyze the mass density and the thickness of biolayers but also to obtain kinetic data.

## E. ATR-FTIR

FTIR uses infrared light to get information on the secondary structure of proteins, notably the presence of α-helices and β-sheets that can be detected at specific positions inside the amide I band of the proteins[90] [Fig. 2(d)]. Furthermore, specific functional groups such as $COO^-$ in carboxylic acids or $SO_3^{2-}$ in sulfated biomolecules can be easily and specifically detected, like specific groups in polysaccharide rings.[91] Different parts of the spectrum are usually distinguished: saccharide ring around 900–1150 $cm^{-1}$, amide I abound from 1500 to 1700 $cm^{-1}$, and H-bonds at 3000–3300 $cm^{-1}$.

The absorbance of biomolecules on surfaces can be followed and quantified using the ATR mode,[92] where the infrared light is passed and guided through a high refractive index substrate (Ge, ZnSe, or Si) in order to create an evanescent wave at the crystal/solution interface where the layer is adsorbing. Multiple reflections enable to increase the sensitivity. Similarly to OWLS but this time with IR light, the penetration depth of this evanescent wave enables to probe the biomolecular adsorption at the surface.

For the quantification, the knowledge of the penetration depth of the evanescent wave, $d_P$,[93] and of the calibration constant K given below are required:

$$d_P = \frac{\lambda}{2\pi n_1 [\sin^2(\theta) - (n_C/n_F)]^2}, \tag{9}$$

with λ, the wavelength of the incident light, $n_F$ and $n_C$, the refractive indices of the ZnSe substrate and the medium, respectively (2.42 and 1.34), and θ the incident angle (45°).

In the case of an infinite medium, the absorbance can be derived as[93]

$$A = K \times C \quad \text{with } K = \frac{n_C}{n_F} \frac{\varepsilon}{\cos\theta} \frac{d_P}{2}, \tag{10}$$

where C is the concentration of the biomolecules in mg/mL and ε is the dielectric permittivity of the medium.

For the amide I peak, $COO^-$ and C–O–S bonds, $d_P$ can vary between ≈900 and 1500 nm,[94] i.e., about 10 times more than for OWLS since λ is much higher in IR than in visible light.

A great advantage of the technique is the robustness and specific chemical signatures of the functional groups. One drawback is the need to work in deuterium oxide ($D_2O$) instead of water due to the strong absorption of water in the amide I range. Also, it is not highly sensitive and requires a few milliliters of solution to pass in the chamber above the crystal. In order to get quantitative information, there is a need to deconvolute the spectra, which requires some processing: the peak positions of the amide I band are first estimated by calculating the secondary derivative of the band [Fig. 2(d′)]. Then, the band is deconvoluted using Lorenzian or Gaussian functions for each subpeak [Fig. 2(d′)]. Finally, the % of each secondary structure is calculated by dividing the area of a given peak by the whole area of the band.

ATR-FTIR was used to probe the secondary structure of insulin adsorbed onto hydrophobic surfaces[63] and to follow the formation of aggregates as a function of time. It was used to study the secondary structure of a growth factor, the BMP-2 trapped in hydrated films and in dry polyelectrolyte films[4] [Figs. 2(d′) and 2(d″)] in view of future application for orthopedic biomaterials. The structural elements were

found to be preserved when BMP-2 was trapped in the biopolymeric film in hydrated conditions and, to a lesser extent, in the dry state.

Absolute quantification of the adsorbed mass is also possible [Eq. (9)], provided that a calibration has been done before, using the same polymers in solution in contact with a nonadsorbing crystal.[95] The adsorbed mass, Γ, which represents a dry mass, can then be quantified. It can be compared to the mass obtained by QCM-D to calculate the percentage of hydration of the layer. Such comparisons have already been done for polyelectrolyte multilayer films.[94,96] The ion pairing in the polyelectrolyte multilayer assemblies can also be deduced.[94,97] Furthermore, the presence of hydrogen bonds in LbL assemblies can be clearly identified in the 2500–3500 $cm^{-1}$ region.[98]

### F. Spectroscopic ellipsometry

Ellipsometry is an optical technique that measures the changes in the polarization of light upon reflection at a planar surface [Fig. 3(a)]. This is typically done as a function of incidence angle or wavelength (or both). The name ellipsometry comes from the fact that polarized light becomes elliptical upon light reflection. Polarized light arriving on the sample can be decomposed in *s* (TE) and *p* (TM) components, oscillating perpendicular and parallel to the plane of incidence, respectively. The amplitude of the *s*-wave and *p*-wave reflected by the sample is normalized to their initial values and denoted as $r_{TE}$ and $r_{TM}$.

The complex reflectance ratio between $r_{TE}$ and $r_{TM}$ is denoted R. Its amplitude and phase shift can be written as a function of two parameters (Ψ, Δ):

$$R = \frac{r^{TM}}{r^{TE}} = \tan\psi \,.\, e^{j\Delta}, \tag{11}$$

with $\Delta = \delta_1 - \delta_2$ ($\delta_1$ is the phase shift before reflection and $\delta_2$ is the phase shift after reflection), measured by ellipsometry.

In SE, the spectra of Ψ and Δ are measured by changing the wavelength of light.[99] However, the parameters Ψ and Δ cannot be directly converted into the optical properties of the film since they depend on several parameters such as film thickness, refractive index, extinction coefficient, surface anisotropy, and surface roughness. The refractive index n depends on λ in a complex manner[100] and needs to be modeled. When the optical constants of the media are well known, it is possible to use the Cauchy method which calculates the real (n) and the imaginary (k) part of the refractive index for a material.[99] The application of models is therefore a drawback of this technique but necessary to calculate $d_A$, $n_A$, and then deduce Γ.

By applying these principles, SE permits to obtain quantitative information on the adsorbed biomasses in liquid environments with a sensitivity that allows to measure thicknesses of a fraction of a molecular layer and the possibility to follow layer deposition in a time-resolved manner (milliseconds).[101] The drawbacks are (i) the analysis of SE data can become complex when detailed information is required or if the investigated films have unknown optical properties[102] and (ii) the lateral resolution of the light beam tends to be in the order of mm. To improve the spatial resolution, imaging ellipsometry has been developed.[103]

This will permit the characterization of more complex substrate–protein interfaces such as multilayer films.[104,105] By controlling the surface density of bioactive proteins, it is possible to distinguish the effect of the type of immobilization at the cellular level; i.e., the cellular effect of a glycosaminoglycan heparan sulfate on the HS-adsorbed BMP-2 bioactivity has been appreciated in comparison to the same surface amount of BMP-2 directly grafted on the surface[106] [Figs. 3(a′) and 3(a″)]. Binding kinetics can also be obtained with SE as it has been demonstrated for tumor necrosis factor-inducible gene 6 protein on a hyaluronic acid film.[107]

### G. Quartz crystal microbalance with dissipation monitoring

QCM-D is an acoustic technique based on the inverse piezoelectric effect [Fig. 3(b)]. A quartz crystal is made oscillating at its resonance frequency *f*. The adsorption or grafting of a layer onto it induces a frequency shift, Δ*f*. Rodahl *et al.*[108] designed a "ring-down" method which cuts the driving circuit and monitors the freely decaying oscillation of the crystal. From fitting the exponential decay curve, the frequency and the energy dissipation are extracted. The damping factor (D), called dissipation, is related to the ratio between the energy dissipated during the period of oscillation ($E_{dissipated}$) and the energy stored in the system ($E_{stored}$).[109]

$$D = \frac{E_{dissipated}}{2\pi E_{stored}}. \tag{12}$$

QCM-D monitors the adsorption process in real time in liquid, providing detailed information about the binding kinetics, and the morphology and stability of thin films made of polymers (natural or synthetic) and proteins.

In the case of a thin and rigid film, Δ*f* is related to the adsorbed mass Δ*m* by the Sauerbrey equation:[110]

$$\Delta m = -\frac{C\Delta f}{n}, \tag{13}$$

where *C* is the mass sensitivity constant (17.7 ng $cm^{-2}$ $Hz^{-1}$ at 5 MHz) and *n* is the overtone number.

For a viscoelastic film, the QCM-D response has been modeled using a Voigt model[111] (i.e., a spring and dashpot in parallel under no slip conditions). It is assumed that the adsorbed layer is homogeneous with a uniform thickness. The frequency changes (Δ*f*) and the dissipation factor changes (Δ*D*) can thus be written as

$$\Delta f \approx -\frac{1}{2\pi\rho_0 d_0}\left\{\frac{\eta_C}{\delta_C} + dA\rho_F\varpi - 2dA\left(\frac{\eta_C}{\delta_C}\right)^2 \frac{\eta_A\varpi^2}{\mu_F^2 + \varpi^2\eta_A^2}\right\} \tag{14}$$

and

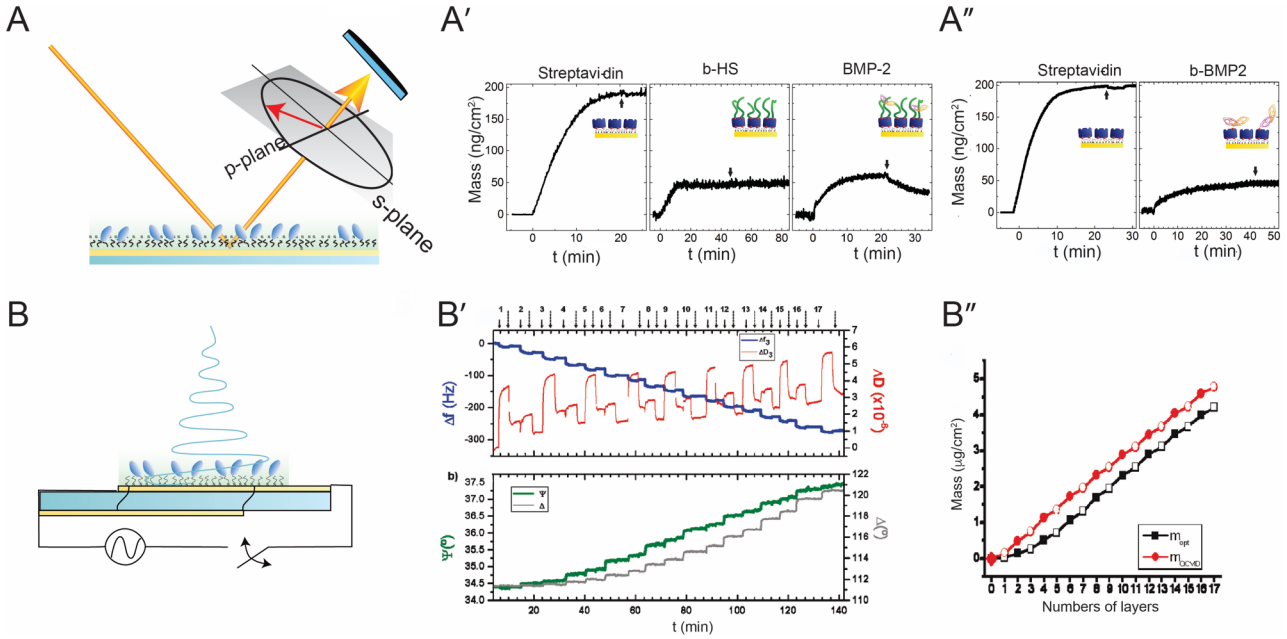


FIG. 3. (a) Spectroscopic ellipsometry general principle. [(a′) and (a″)] Spectroscopic measurements of the mass adsorption of biomolecules with time: (a′) sequential adsorption of streptavidin, biotinylated heparan sulfate, and BMP-2; (a″) mass of streptavidin coated with biotinylated BMP-2 (b-BMP-2). Start of buffer rinse is indicated by arrows. Adapted with permission from Migliorini *et al.*, Adv. Biosyst. **1**, 1600041 (2017). Copyright 2017, WILEY-VCH Verlag GmbH & Co. (b) QCM-D schematic representation of the principle. [(b′) and (b″)] Combined QCM-D and SE to follow real time layer-by-layer assembly. (b′) Assembly of 17 polyelectrolyte layers followed *in situ* by the combined QCM-D/ellipsometry device showing two graphs: on top, the QCM-D response $\Delta f$ and $\Delta D$ vs time for a selected overtone ($i = 3$) and at the bottom, ellipsometric response $\psi$ and $\Delta$ vs time for a selected wavelength ($\lambda = 632.5$ nm). The starting time of each deposition step and rinses are indicated by solid and dashed arrows, respectively, together with the step number. (b″) Adsorbed mass as a function of the number of deposited layers measured via the two experimental techniques: $\Gamma_{opt}$ (squares, measured by ellipsometry) reflects the pure polymer mass while $\Gamma_{QCM}$ (circles, measured by QCM-D) includes solvent in the film. Both measured $\Gamma$ exhibit an approximately linear growth trend. Reproduced with permission from Ramos *et al.*, Macromolecules **43**, 9063 (2010). Copyright 2010, American Chemical Society.

$$\Delta D \approx -\frac{1}{\pi f \rho_0 d_0}\left\{\frac{\eta_C}{\delta_C} + 2dA\left(\frac{\eta_C}{\delta_C}\right)^2 \frac{\eta_A \varpi^2}{\mu_A^2 + \varpi^2 \eta_A^2}\right\}, \quad (15)$$

where $\omega$ is the angular frequency of the oscillation, and $\rho_0$ and $h_0$ are the density and thickness of the crystal, respectively. The viscosity of the bulk liquid is $\eta_C$, $\delta_C = (2\eta_C/\rho_C\omega)^{1/2}$ is the viscous penetration depth of the shear wave in the bulk liquid, and $\rho_C$ is the liquid density. The thickness, density, viscosity, and elastic shear modulus of the adsorbed layer are represented by $d_A$, $\rho_A$, $\eta_A$, and $\mu_A$, respectively.

By assuming the density and viscosity of the bulk liquid ($\rho_C$ and $\eta_C$ are 1000 kg m$^{-3}$ and 1 mPa s, respectively) and a fixed density of the layer ($\rho_F = 1009$ kg m$^{-3}$), the QTOOLS software (Qsense, Gotenborg, Sweden) estimates the thickness, viscosity, and shear modulus of the adsorbed layer. Another robust method, alternative to Voigt, for QCM-D data of homogeneous viscoelastic films has been published.[112,113] It considers the film as a viscoelastic material characterized by a shear complex modulus G($\omega$). For a more complete explanation on the viscoelastic and mechanic measurements with QCM-D, refer to Johannsmann.[114]

QCM-D measures the mass of biomolecules coupled with the solvent (often water) in the film. To obtain quantitative information on the dried adsorbed mass, it is appropriate to combine it with optical techniques such as OWLS,[115] SE in liquid,[116] or ATR-FTIR.[94] The combined QCM-D and SE setup has been used for the first time to characterize the deposition of polymeric layers in layer-by-layer film deposition[116] [Fig. 3(b)]. This process has already been characterized by QCM-D; however, the authors wanted to understand how much the deposition of a new polyelectrolyte layer would affect the content of water of the previously assembled layers. The combination of QCM-D and SE in the same device permits to follow in real time the solvent-dependent growth of the LbL film [Fig. 3(b)] and to calculate the hydration of the multilayer film by comparing the optical mass to the QCM-D mass [Fig. 3(b)].[116]

## H. Atomic force microscopy

AFM is a scanning probe technique that uses the tip of a cantilever to probe the surface by measuring the interaction forces between the tip and the surface[117] (Fig. 4). When the AFM tip approaches the sample, it experiences attractive forces due to van-der-Waals, capillary forces, and, once in contact with the sample, repulsive forces generated by the electron clouds around atoms. There are two possible working modes: contact and intermittent mode. In contact mode, the distance between the tip and the surface is kept constant and the interaction forces are measured; alternatively, the force is fixed to a certain value and the distances between the tip and the surface are varied to keep the force value constant. This imaging mode is rather appropriate for samples with low

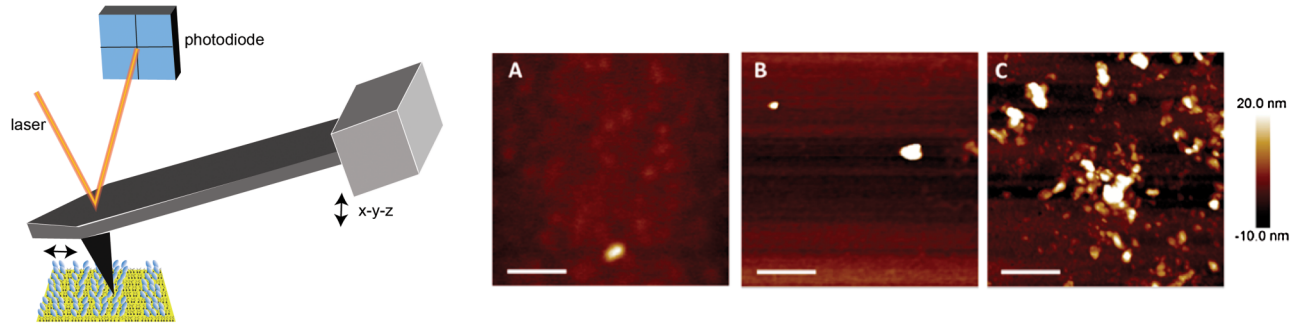


FIG. 4. AFM schematic representation of the principle of AFM imaging. [(a)–(c)] AFM images of insulin prenuclei formed on a hydrophobic surface upon incubation with (a) aggregative peptide alone, (b) insulin solution without peptide, and (c) insulin solution with aggregative peptide. The scale bar represents 500 nm. Reproduced with permission from Chouchane *et al.*, J. Phys. Chem. B **119**, 10543 (2015). Copyright 2015, American Chemical Society.

surface roughness. In the intermittent mode, the tip is made oscillating at a given frequency and the amplitude of the oscillating cantilever is recorded. The interaction force between the tip and the surface influences this amplitude. In the intermittent contact mode (or tapping mode), the tip goes in contact with the sample. In the noncontact mode, the tip is positioned at a given distance of the surface, which depends on the tip/surface interaction force that is set by the user to a given value. The precise control of the tip position is ensured via a feedback control loop. In both contact mode and intermittent mode, a feedback loop moves the tip up and down to keep the interaction force constant, providing direct information on the tip/surface distance, and thus the height of the sample. Tapping mode is the preferred working mode when delicate objects such as proteins are to be imaged. AFM can be performed in air or in liquid. In this latter case, care should be taken that the experimental conditions are stabilized (working in buffer and at perfectly controlled temperature) in order to avoid signal drift. It is often used to image surface topography and deduce surface roughness at the nanometer scale as well as to image protein aggregates.[118]

AFM can be used to image adsorbed molecules on a surface, to appreciate their size, homogeneity, and density which can be relevant to understand their adsorption kinetics. Human insulin amyloid aggregation is triggered by its adsorption on hydrophobic surfaces. The kinetics is characterized by an important lag phase during which aggregative nuclei form on the surface. This lag phase can be dramatically shortened in the presence of substoichiometric amounts of aggregative peptides (LK9) in solution.[119] Figure 4(c) shows that this acceleration goes in pair with the rapid formation of numerous surface-adsorbed nuclei which are absent when peptide [Fig. 4(a)] or insulin [Fig. 4(b)] are incubated alone with the hydrophobic surface. The acceleration is thus due to a surface-linked phenomenon, namely the preferential formation of adsorbed aggregation nuclei.

Soft and hydrated surfaces, such as those made of polymer brushes, are usually more difficult to image since they are prone to uncontrolled tip/surface interactions and displacement by the tip. AFM has been widely used to image protein aggregation at surfaces,[120] fibril formation,[121] polyelectrolyte brushes, and polyelectrolyte multilayer films.[75]

In addition to surface imaging, AFM can measure force–distance curves and provide information on interaction forces. It is possible to chemically modify the tip in order to measure specific interaction forces at single molecular level[122] or at cell–cell or cell–substrate level.[123,124] A colloidal probe attached to the tip can also be used to locally perform nanoindentations and, using an appropriate model, to fit the force/distance curves, to quantitatively estimate an apparent Young's modulus.[125,126]

There are a few drawbacks of the technique: being a scanning probe technique, image acquisition requires at least several minutes or tens of minutes depending on the expected resolution, a drawback that can be improved by using high-speed AFM.[117] The signal acquisition is also affected by thermal noise fluctuations and high resolution imaging can be obtained only in very well controlled environmental conditions. The proximity of the tip with the surface may lead to tip contamination or to unwanted motion of the adsorbed biomolecules.

## IV. SUMMARY AND CONCLUSIONS

Characterizing the adsorption of biomolecules on solid surfaces remains challenging because of the very small amounts of adsorbed material to be detected, the inherent difficulties to sense at an interface without interference from the solution and the concomitance of several molecular phenomena (adsorption, desorption, conformational changes, and rearrangements). The complete description of molecular surface adsorption needs with no doubt input from multiple, complementary surface sensing techniques that are either optical or acoustic and should ideally bring together data on the amount, distribution, conformation, and stability of surface-adsorbed molecules.

Most techniques have similar sensitivities, but allow more or less flexibility in terms of type of surface or functionalization, parallel experimental runs, and ease of use (Table I). However, each method is more adequate to obtain a certain type of parameter. In particular, the most accurate methods to measure the dry mass are SE, OWLS, and DPI while it is QCM-D for the wet mass. Besides, the mechanical properties of soft biomolecules can be measured during their surface adsorption using QCM-D. SPR has been mostly developed

to study the binding kinetics of biomolecules on a substrate. ATR-FTIR is used to gain information on molecular conformational changes. Finally, the spatial organization of biomolecules can be imaged using AFM. It should be noted that there are limitations in the models that are currently used to get quantitative data. It would be nice if more efforts could be done to take into account the full equations, not their approximated form to very small thicknesses, and layer anisotropy, and to implant these models in the softwares used for data analysis.

Currently, there is a trend to develop the techniques and to combine several techniques in a single instrument in order to gain further insight into the nature and characteristics of the adsorbed molecular species. For example, OWLS was combined with ellipsometry[80] and SPR with mass spectroscopy.[68]

In all the presented techniques, efforts are also made to gain in sensitivity, throughput, and other important parameters such as minimization of sample volume or even sample recycling. New techniques are currently being developed such as biolayer interferometry that can be used at high throughput[127,128] and wet surface-enhanced ellipsometric contrast microscopy[129] to image surface adsorption with nanometric z resolution. The progress in experimental techniques also nourishes modeling and simulation of molecular surface adsorption, which contribute to our understanding of these complex multiscale phenomena.[130]

## ACKNOWLEDGMENTS

This work was funded by the Institut Universitaire de France (C.P. being a senior member of the Institute), ANR PIRE REACT (No. ANR-15-PIRE-0001-02), Fondation Recherche Médicale (No. DEQ20170336746), and ANR CODECIDE (No. ANR-17-CE13-022). The authors thank Pascal Picart (Univ. Le Mans) and Jérome Dejeu (University of Grenoble Alpes) for technical advice regarding the optical equations. This paper is dedicated to the memory of Professor Helmuth Moehwald, who was the director of the Max Planck Institute of Colloids and Interfaces, Potsdam, Germany, and died on March 27, 2018 at the age of 72. He was truly passionate for science and was communicating his passion to younger scientists. He was an extremely open minded person, who was highly innovative in his projects and had a scientific vision. Although she never directly studied under his supervision, he was a mentor for C.P. Together with Thomas Zemb, he opened to her the doors of the French/German network for Colloids and Interfaces in 2003. This was a wonderful opportunity in her scientific career and was greatly inspiring.

[1]A. K. Trilling, M. M. Harmsen, V. J. Ruigrok, H. Zuilhof, and J. Beekwilder, Biosens. Bioelectron. **40**, 219 (2013).
[2]M. C. Manning, D. K. Chou, B. M. Murphy, R. W. Payne, and D. S. Katayama, Pharm. Res. **27**, 544 (2010).
[3]C. Pinholt, R. A. Hartvig, N. J. Medlicott, and L. Jorgensen, Expert Opin. Drug Deliv. **8**, 949 (2011).
[4]F. Gilde, O. Maniti, R. Guillot, J. F. Mano, D. Logeart-Avramoglou, F. Sailhan, and C. Picart, Biomacromolecules **13**, 3620 (2012).
[5]E. Migliorini, A. Valat, C. Picart, and E. A. Cavalcanti-Adam, Cytokine Growth Factor Rev. **27**, 43 (2016).
[6]Q. Lubart, H. Vitet, F. Dalonneau, A. Le Roy, M. Kowalski, M. Lourdin, C. Ebel, M. Weidenhaupt, and C. Picart, Biophy. J. **114**, 98 (2018).
[7]K. Carvalho, L. Ramos, C. Roy, and C. Picart, Biophys. J. **95**, 4348 (2008).
[8]N. Yandrapalli, Q. Lubart, H. S. Tanwar, C. Picart, J. Mak, D. Muriaux, and C. Favard, Sci. Rep. **6**, 39332 (2016).
[9]E. Hamard-Peron, F. Juillard, J. S. Saad, C. Roy, P. Roingeard, M. F. Summers, J. L. Darlix, C. Picart, and D. Muriaux, J. Virol. **84**, 503 (2010).
[10]A. Bretscher, K. Edwards, and R. G. Fehon, Nat. Rev. Mol. Cell Biol. **3**, 586 (2002).
[11]S. Vanni, H. Hirose, H. Barelli, B. Antonny, and R. Gautier, Nat. Commun. **5**, 4916 (2014).
[12]A. Lundgren, B. J. Fast, S. Block, B. Agnarsson, E. Reimhult, A. Gunnarsson, and F. Hook, Nano Lett. **18**, 381 (2018).
[13]E. Sackmann, Biochim. Biophys. Acta **1853**, 3132 (2015).
[14]M. Rabe, D. Verdes, and S. Seeger, Adv. Colloid Interface Sci. **162**, 87 (2011).
[15]A. A. Khorasani, J. L. Weaver, and C. Salvador-Morales, Int. J. Nanomed. **9**, 5729 (2014).
[16]K. Nakanishi, T. Sakiyama, and K. Imamura, J. Biosci. Bioeng. **91**, 233 (2001).
[17]P. Roach, D. Farrar, and C. C. Perry, J. Am. Chem. Soc. **127**, 8168 (2005).
[18]L. Vroman and A. L. Adamas, Surf. Sci. **16**, 438 (1969).
[19]T. Arai and W. Norde, Colloids Surf. **51**, 1 (1990).
[20]C. A. Keller and B. Kasemo, Biophys. J. **75**, 1397 (1998).
[21]S. R. Tabaei, J. A. Jackman, S. O. Kim, V. P. Zhdanov, and N. J. Cho, Langmuir **31**, 3125 (2015).
[22]W. G. Ellenbroek, Y. H. Wang, D. A. Christian, D. E. Discher, P. A. Janmey, and A. J. Liu, Biophys. J. **101**, 2178 (2011).
[23]B. G. Keselowsky, D. M. Collard, A. J. Garcia, and J. Biomed, Mater. Res. Part A **66A**, 247 (2003).
[24]J. O. Zoppe, N. C. Ataman, P. Mocny, J. Wang, J. Moraes, and H. A. Klok, Chem. Rev. **117**, 1105 (2017).
[25]X. Laloyaux, E. Fautre, T. Blin, V. Purohit, J. Leprince, T. Jouenne, A. M. Jonas, and K. Glinel, Adv. Mater. **22**, 5024 (2010).
[26]J. J. Richardson, M. Bjornmalm, and F. Caruso, Science **348**, aaa2491 (2015).
[27]S. I. Jeon, J. H. Lee, J. D. Andrade, and P. G. Degennes, J. Colloid Interface Sci. **142**, 149 (1991).
[28]R. P. Richter, R. Berat, and A. R. Brisson, Langmuir **22**, 3497 (2006).
[29]M. J. Kim, B. Lee, K. Yang, J. Park, S. Jeon, S. H. Um, D. I. Kim, S. G. Im, and S. W. Cho, Biomaterials **34**, 7236 (2013).
[30]C. Schulte, A. Podesta, C. Lenardi, G. Tedeschi, and P. Milani, Acc. Chem. Res. **50**, 231 (2017).
[31]M. Kastantin, B. B. Langdon, and D. K. Schwartz, Adv. Colloid Interface Sci. **207**, 240 (2014).
[32]M. Rabe, D. Verdes, J. Zimmermann, and S. Seeger, J. Phys. Chem. B **112**, 13971 (2008).
[33]R. C. Chatelier and A. P. Minton, Biophys. J. **71**, 2367 (1996).
[34]M. Holmberg and X. Hou, Langmuir **25**, 2081 (2009).
[35]A. P. Minton, Biophys. J. **80**, 1641 (2001).
[36]V. Sluzky, J. A. Tamada, A. M. Klibanov, and R. Langer, Proc. Natl. Acad. Sci. U.S.A. **88**, 9377 (1991).
[37]T. Ballet, F. Brukert, P. Mangiagalli, C. Bureau, L. Boulange, L. Nault, T. Perret, and M. Weidenhaupt, Biochemistry **51**, 2172 (2012).
[38]C. J. Roberts, Trends Biotechnol. **32**, 372 (2014).
[39]W. Norde, F. Macritchie, G. Nowicka, and J. Lyklema, J. Colloid Interface Sci. **112**, 447 (1986).
[40]T. Vermonden, C. E. Giacomelli, and W. Norde, Langmuir **17**, 3734 (2001).
[41]J. S. Bee, M. Davis, E. Freund, J. F. Carpenter, and T. W. Randolph, Biotechnol. Bioeng. **105**, 121 (2010).
[42]E. Gurdak, C. C. Dupont-Gillain, J. Booth, C. J. Roberts, and P. G. Rouxhet, Langmuir **21**, 10684 (2005).
[43]X. B. Zhao, F. Pan, and J. R. Lu, J. R. Soc. Interface **6**, S659 (2009).
[44]S. M. Kilbey and J. F. Ankner, Curr. Opin. Colloid Interface Sci. **17**, 83 (2012).
[45]M. Kulkarni, A. Mazare, J. Park, E. Gongadze, M. S. Killian, S. Kralj, K. von der Mark, A. Iglic, and P. Schmuki, Acta Biomater. **45**, 357 (2016).
[46]M. Born and E. Wolf, *Principles of Optics: Electromagnetic Theory of Propagation, Interference and Diffraction of Light*, 7th ed. (Cambridge University, Cambridge, 1999).

[47]J. A. De Feijter, J. Benjamins, and F. A. Veer, Biopolymers **17**, 1759 (1978).
[48]H. Zhao, P. H. Brown, and P. Schuck, Biophys. J. **100**, 2309 (2011).
[49]E. Engvall and P. Perlmann, Immunochemistry **8**, 871 (1971).
[50]P. J. Tighe, R. R. Ryder, I. Todd, and L. C. Fairclough, Proteomics Clin. Appl. **9**, 406 (2015).
[51]S. Delshadi *et al.*, Bioanalysis **9**, 517 (2017).
[52]D. M. Rissin *et al.*, Nat. Biotechnol. **28**, 595 (2010).
[53]A. Olaru, C. Bala, N. Jaffrezic-Renault, and H. Y. Aboul-Enein, Crit. Rev. Anal. Chem. **45**, 97 (2015).
[54]M. Puiu and C. Bala, Sensors **16**, 15 (2016).
[55]E. Mauriz, M. C. Garcia-Fernandez, and L. M. Lechuga, TrAC Trends Anal. Chem. **79**, 191 (2016).
[56]M. Yamamoto, Vol. 2018 (Kyoto, Japan, 2009).
[57]Y. Tang, X. Zeng, and J. Liang, J. Chem. Educ. **87**, 742 (2010).
[58]A. B. Biacore (GE Healthcare Bio-Sciences AB, Uppsala, 2003).
[59]H. H. Nguyen, J. Park, S. Kang, and M. Kim, Sensors **15**, 10481 (2015).
[60]X. Li, M. Wang, L. Wang, X. Shi, Y. Xu, B. Song, and H. Chen, Langmuir **29**, 1122 (2013).
[61]M. Vuoriluoto, H. Orelma, B. Zhu, L. S. Johansson, and O. J. Rojas, ACS Appl. Mater. Interfaces **8**, 5668 (2016).
[62]P. Lavalle, C. Gergely, F. J. G. Cuisinier, G. Decher, P. Schaaf, J. C. Voegel, and C. Picart, Macromolecules **35**, 4458 (2002).
[63]L. Nault, P. Guo, B. Jain, Y. Brechet, F. Bruckert, and M. Weidenhaupt, Acta Biomater. **9**, 5070 (2013).
[64]N. Nath and A. Chilkoti, Anal. Chem. **76**, 5370 (2004).
[65]S. Unser, I. Bruzas, J. He, and L. Sagle, Sensors **15**, 15684 (2015).
[66]E. Petryayeva and U. J. Krull, Anal. Chim. Acta **706**, 8 (2011).
[67]B. Huang, F. Yu, and R. N. Zare, Anal. Chem. **79**, 2979 (2007).
[68]D. Nedelkov, Methods Mol. Biol. **627**, 261 (2010).
[69]B. D. Gupta, A. M. Shrivastav, and S. P. Usha, Sensors **16**, 33 (2016).
[70]B. Kovacs, D. Patko, A. Klein, B. Kakasi, A. Saftics, S. Kurunczi, F. Vonderviszt, and R. Horvath, Sens. Actuators B: Chem. **257**, 839 (2018).
[71]J. F. Popplewell, M. J. Swann, Y. Ahmed, J. E. Turnbull, and D. G. Fernig, Chembiochem **10**, 1218 (2009).
[72]K. Tiefenthaler and W. Lukosz, J. Opt. Soc. Am. B **6**, 209 (1989).
[73]C. Picart, C. Gergely, Y. Arntz, P. Schaaf, J.-C. Voegel, F. G. Cuisinier, and B. Senger, Biosens. Bioelectron. **20**, 553 (2004).
[74]A. Saftics *et al.*, Appl. Surf. Sci. **281**, 66 (2013).
[75]C. Picart, P. Lavalle, P. Hubert, F. J. G. Cuisinier, G. Decher, P. Schaaf, and J.-C. Voegel, Langmuir **17**, 7414 (2001).
[76]T. Gillich, E. M. Benetti, E. Rakhmatullina, R. Konradi, W. Li, A. Zhang, A. D. Schluter, and M. Textor, J. Am. Chem. Soc. **133**, 10940 (2011).
[77]K. Abdelkebir, F. Gaudiere, S. Morin-Grognet, G. Coquerel, B. Labat, H. Atmani, and G. Ladam, Soft Matter **7**, 9197 (2011).
[78]R. Horvath and J. J. Ramsden, Langmuir **23**, 9330 (2007).
[79]B. Peter *et al.*, Sci. Rep. **7**, 16 (2017).
[80]E. Agocs *et al.*, Appl. Surf. Sci. **421**, 289 (2017).
[81]G. H. Cross, Y. T. Ren, and N. J. Freeman, J. Appl. Phys. **86**, 6483 (1999).
[82]G. H. Cross, A. A. Reeves, S. Brand, J. F. Popplewell, L. L. Peel, M. J. Swann, and N. J. Freeman, Biosens. Bioelectron. **19**, 383 (2003).
[83]G. H. Cross, A. Reeves, S. Brand, M. J. Swann, L. L. Peel, N. J. Freeman, and J. R. Lu, J. Phys. D: Appl. Phys. **37**, 74 (2004).
[84]P. Kozma, F. Kehl, E. Ehrentreich-Forster, C. Stamm, and F. F. Bier, Biosens. Bioelectron. **58**, 287 (2014).
[85]S. Ricard-Blum, L. L. Peel, F. Ruggiero, and N. J. Freeman, Anal. Biochem. **352**, 252 (2006).
[86]J. Escorihuela, M. A. Gonzalez-Martinez, J. L. Lopez-Paz, R. Puchades, A. Maquieira, and D. Gimenez-Romero, Chem. Rev. **115**, 265 (2015).
[87]T. H. Lee, D. J. Hirst, and M. I. Aguilar, Biochim. Biophys. Acta Biomembr. **1848**, 1868 (2015).
[88]K. Karim, J. D. Taylor, D. C. Cullen, M. J. Swann, and N. J. Freeman, Anal. Chem. **79**, 3023 (2007).
[89]J. Zhai, T. H. Lee, D. H. Small, and M. I. Aguilar, Biochemistry **51**, 1070 (2012).
[90]A. Barth and C. Zscherp, Q. Rev. Biophys. **35**, 369 (2002).
[91]K. Haxaire, Y. Marechal, M. Milas, and M. Rinaudo, Biopolymers **72**, 10 (2003).
[92]P. Schwinté, J.-C. Voegel, C. Picart, Y. Haikel, P. Schaaf, and B. Szalontai, J. Phys. Chem. B **105**, 11906 (2001).
[93]N. J. Harrick, J. Opt. Soc. A **55**, 851 (1965).
[94]T. Crouzier and C. Picart, Biomacromolecules **10**, 433 (2009).
[95]S. Sukhishvili and S. Granick, Macromolecules **35**, 301 (2002).
[96]T. T. Ho, K. E. Bremmell, M. Krasowska, S. V. MacWilliams, C. J. Richard, D. N. Stringer, and D. A. Beattie, Langmuir **31**, 11249 (2015).
[97]J. Almodovar, L. W. Place, J. Gogolski, K. Erickson, and M. J. Kipper, Biomacromolecules **12**, 2755 (2011).
[98]L. Shen, P. Chaudouet, J. Ji, and C. Picart, Biomacromolecules **12**, 1322 (2011).
[99]F. Hiroyuki, *Spectroscopic Ellipsometry: Principles and Applications* (Wiley, Hoboken, NJ, 2007).
[100]J. N. Hilfiker, N. Singh, T. Tiwald, D. Convey, S. M. Smith, J. H. Baker, and H. G. Tompkins, Thin Solid Films **516**, 7979 (2008).
[101]R. W. Collins, I. An, H. V. Nguyen, and Y. W. Lu, Thin Solid Films **233**, 244 (1993).
[102]H. Arwin, Thin Solid Films **377**, 48 (2000).
[103]S. Funke, B. Miller, E. Parzinger, P. Thiesen, A. W. Holleitner, and U. Wurstbauer, J. Phys. Condens. Matter **28**, 12 (2016).
[104]N. B. Eisele, S. Frey, J. Piehler, D. Gorlich, and R. P. Richter, EMBO Rep. **11**, 366 (2010).
[105]E. Migliorini, D. Thakar, R. Sadir, T. Pleiner, F. Baleux, H. Lortat-Jacob, L. Coche-Guerente, and R. P. Richter, Biomaterials **35**, 8903 (2014).
[106]E. Migliorini, P. Horn, T. Haraszti, S. Wegner, C. Hiepen, P. Knaus, R. Richter, and E. Cavalcanti-Adam, Adv. Biosyst. **1**, 1600041 (2017).
[107]N. S. Baranova, E. Nileback, F. M. Haller, D. C. Briggs, S. Svedhem, A. J. Day, and R. P. Richter, J. Biol. Chem. **286**, 25675 (2011).
[108]M. Rodahl, F. Hook, A. Krozer, P. Brzezinski, and B. Kasemo, Rev. Sci. Instrum. **66**, 3924 (1995).
[109]M. C. Dixon, J. Biomol. Tech. **19**, 151 (2008), see https://www.ncbi.nlm.nih.gov/pmc/articles/PMC2563918/.
[110]G. Sauerbrey, Zeitschrift fur Physik **155**, 206 (1959).
[111]M. V. Voinova, M. Rodahl, M. Jonson, and B. Kasemo, Phys. Scr. **59**, 391 (1999).
[112]I. Reviakine, D. Johannsmann, and R. P. Richter, Anal. Chem. **83**, 8838 (2011).
[113]M. V. Voinova, M. Jonson, and B. Kasemo, Biosens. Bioelectron. **17**, 835 (2002).
[114]D. Johannsmann, Phys. Chem. Chem. Phys. **10**, 4516 (2008).
[115]F. Hook *et al.*, Colloid Surf. B **24**, 155 (2002).
[116]J. J. I. Ramos, S. Stahl, R. P. Richter, and S. E. Moya, Macromolecules **43**, 9063 (2010).
[117]Y. F. Dufrene, T. Ando, R. Garcia, D. Alsteens, D. Martinez-Martin, A. Engel, C. Gerber, and D. J. Muller, Nat. Nanotechnol. **12**, 295 (2017).
[118]G. Wei, Z. Q. Su, N. P. Reynolds, P. Arosio, I. W. Hamley, E. Gazit, and R. Mezzenga, Chem. Soc. Rev. **46**, 4661 (2017).
[119]K. Chouchane, C. Vendrely, M. Amari, K. Moreaux, F. Bruckert, and M. Weidenhaupt, J. Phys. Chem. B **119**, 10543 (2015).
[120]S. A. Mari, S. Wegmann, K. Tepper, B. T. Hyman, E. M. Mandelkow, E. Mandelkow, and D. J. Muller, Nano Lett. **18**, 3271 (2018).
[121]J. Adamcik, J. M. Jung, J. Flakowski, P. De Los Rios, G. Dietler, and R. Mezzenga, Nat. Nanotechnol. **5**, 423 (2010).
[122]M. Rief, M. Gautel, F. Oesterhelt, J. M. Fernandez, and H. E. Gaub, Science **276**, 1109 (1997).
[123]J. Helenius, C. P. Heisenberg, H. E. Gaub, and D. J. Muller, J. Cell Sci. **121**, 1785 (2008).
[124]E. Migliorini, J. Ban, G. Grenci, L. Andolfi, A. Pozzato, M. Tormen, V. Torre, and M. Lazzarino, Biotechnol. Bioeng. **110**, 2301 (2013).
[125]Y. B. Lu *et al.*, Proc. Natl. Acad. Sci. U.S.A. **103**, 17759 (2006).
[126]L. Amin, E. Ercolini, R. Shahapure, E. Migliorini, and V. Torre, Biophys. J. **102**, 2451 (2012).
[127]Y. Abdiche, D. Malashock, A. Pinkerton, and J. Pons, Anal. Biochem. **377**, 209 (2008).
[128]V. Kamat and A. Rafique, Anal. Biochem. **536**, 16 (2017).
[129]A. Ducret, M. P. Valignat, F. Mouhamar, T. Mignot, and O. Theodoly, Proc. Natl. Acad. Sci. U.S.A. **109**, 10036 (2012).
[130]M. Ozboyaci, D. B. Kokh, S. Corni, and R. C. Wade, Q. Rev. Biophys. **49**, e4 (2016).
[131]J. Voros, J. J. Ramsden, G. Csucs, I. Szendro, S. M. De Paul, M. Textor, and N. D. Spencer, Biomaterials **23**, 3699 (2002).
[132]N. J. Harrick, *Internal Reflection Spectroscopy* (Interscience, Olney, UK, 1967).

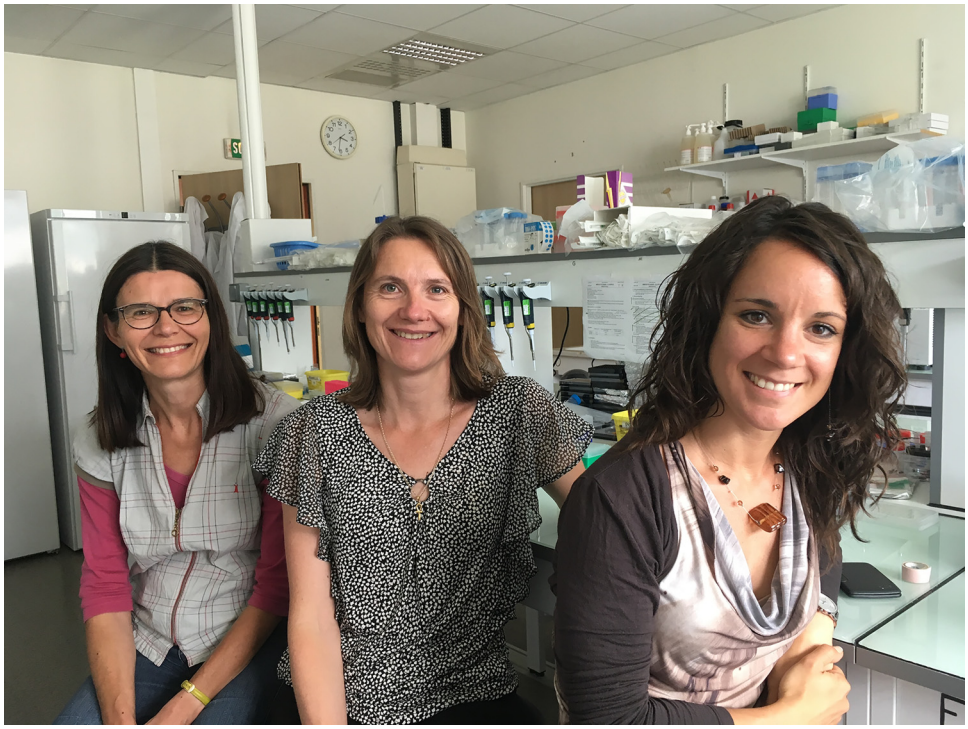

**Catherine Picart** received an engineering degree in Material Science from Grenoble Institute of Technology, a Master in Biomedical Engineering in 1994, and a Ph.D. in Biomedical Engineering from the University Joseph Fourier (Grenoble) in 1997. After postdoctoral training in Bioengineering at the University of Pennsylvania in Philadelphia, she was appointed as an Assistant Professor in Materials/Biomaterials at the Université Louis Pasteur in Strasbourg in 1998. From 2004 to 2008, she was an Associate Professor at the University of Montpellier 2, Department of Biology and Health, where she also became a Junior Member of the "Institut Universitaire de France" (2006–2011). She is presently a Full Professor in Bioengineering/Biomaterials at Grenoble Institute of Technology and a Senior Member of the Institut Universitaire de France (2016–2021). She is working at the Laboratory of Physical Engineering (LMGP) in Minatec in Grenoble in the "Interfaces between Materials and Biological Matter" (IMBM) team (http://www.lmgp.grenoble-inp.fr). She received an ERC Starting Grant at the consolidator stage in 2010 (Biomim), three ERC Proof of Concept grants in 2012 (Oscodi), 2015 (Bioactivecoatings), and 2017 (Regenerbone), and was awarded the CNRS Silver Medal in 2016. Over the years, she has been working on cellular biophysics and biomimetism, advanced materials, and tissue engineering with applications to muscle, bone, and cancer. She is author of 128 publications, 10 review papers in multidisciplinary journals on materials science, biomaterials, and biophysics. She is currently member of the Editorial Advisory Boards of *Advanced Healthcare Materials*, *Tissue Engineering*, *Acta Biomaterialia*, and *Biointerphases* and was previously EAB Member of *ACS Applied Materials and Interfaces*.

According to her: "What I like most in my career is the freedom to think and propose new ideas. I see research projects and papers as a jigsaw, for which you progressively put the different pieces in place, and assemble them so that they form a coherent picture. Initially, your ideas may be a bit blurry but progressively, you form something which makes sense and you create a story. Science is also a team work since different people in a team or collaborators are contributing to assemble the pieces. Also, it is a profound happiness to see the young scientists growing in science, meaning that they progressively enter into their research projects, gain experimental skills and other soft skills, including writing and communication. At some point, they surpass you and manage to go far beyond what was initially planned. It is also rewarding to see their progression in their career, whether academic or nonacademic. Finally, I would like to give an advice to younger researchers: believe in what you are doing, be persistent and don't give up. You need to have a final goal and stick to it. Doing research is like running a marathon: it is a long run and you need to manage your efforts along the road. It is important not to start too fast, since you can burn your wings."

**Elisa Migliorini** is a CNRS researcher since 2017 and works at the LMGP in Minatec in Grenoble, France, in the IMBM team (http://www.lmgp.grenoble-inp.fr). She obtained her Ph.D. in Nanotechnology at the University of Trieste, Italy, in 2012. From 2012 to 2014, she was a postdoctoral fellow at the University of Grenoble Alpes and collaborated with the lab of Prof Richter in San Sebastian, Spain. In 2015, she obtained a Marie-Sklodowska-Curie postdoctoral fellowship to work at the Max Planck Institute for intelligent systems in Stuttgart, Germany. Her research focuses on the

interface between cells and a material substrate. In particular, she aims to control the chemical functionalization in a way to mimic selected aspects of the extracellular matrix, notably the presentation of growth factors and sugars named glycosaminoglycans. She is an author of 16 peer-reviewed papers.

**Marianne Weidenhaupt** is an Associate Professor at Grenoble INP since 2006 and is working at the LMGP in Minatec in Grenoble, France, in the IMBM team (http://www.lmgp.grenoble-inp.fr). She received her Ph.D. from ETH Zurich in 1996 and worked as a postdoctoral fellow at CEA and EMBL in Grenoble, France. She is a trained molecular biologist and biochemist and is currently studying protein adsorption and aggregation at interfaces in the context of therapeutic protein stability. She directs collaborative projects with industrial partners (pharmaceutical industry, and drug reconstitution and delivery systems). She is an author of 32 peer-reviewed papers and 2 patents.